Biochimica et Biophysica Acta 1797 (2010) 262–271

Contents lists available at ScienceDirect

Biochimica et Biophysica Acta

journal homepage: www.elsevier.com/locate/bbabio

Dual role of FMN in flavodoxin function: Electron transfer cofactor and modulation of the protein–protein interaction surface

Susana Frago [a], Isaias Lans [a], José A. Navarro [b], Manuel Hervás [b], Dale E. Edmondson [c], Miguel A. De la Rosa [b], Carlos Gómez-Moreno [a], Stephen G. Mayhew [d], Milagros Medina [a,*]

[a] Departamento de Bioquímica y Biología Molecular y Celular, Facultad de Ciencias, and Institute of Biocomputation and Physics of Complex Systems (BIFI). Universidad de Zaragoza, 50009 Zaragoza, Spain
[b] Instituto de Bioquímica Vegetal y Fotosíntesis, Universidad de Sevilla and CSIC, 41092 Sevilla, Spain
[c] Department of Biochemistry, Emory University School of Medicine, Atlanta, GA 30322, USA
[d] UCD School of Biomolecular and Biomedical Science, Conway Institute for Biomolecular and Biomedical Research, University College Dublin, Belfield, Dublin 4, Ireland

ARTICLE INFO

Article history:
Received 22 September 2009
Received in revised form 29 October 2009
Accepted 30 October 2009
Available online 10 November 2009

Keywords:
Flavodoxin
Reduction potential
FMN analogues
Photosystem I
Protein-protein interaction
Electron transfer
Ferredoxin-NADP$^+$ reductase

ABSTRACT

Flavodoxin (Fld) replaces Ferredoxin (Fd) as electron carrier from Photosystem I (PSI) to Ferredoxin-NADP$^+$ reductase (FNR). A number of *Anabaena* Fld (*An*Fld) variants with replacements at the interaction surface with FNR and PSI indicated that neither polar nor hydrophobic residues resulted critical for the interactions, particularly with FNR. This suggests that the solvent exposed benzenoid surface of the Fld FMN cofactor might contribute to it. FMN has been replaced with analogues in which its 7- and/or 8-methyl groups have been replaced by chlorine and/or hydrogen. The oxidised Fld variants accept electrons from reduced FNR more efficiently than Fld, as expected from their less negative midpoint potential. However, processes with PSI (including reduction of Fld semiquinone by PSI, described here for the first time) are impeded at the steps that involve complex re-arrangement and electron transfer (ET). The groups introduced, particularly chlorine, have an electron withdrawal effect on the pyrazine and pyrimidine rings of FMN. These changes are reflected in the magnitude and orientation of the molecular dipole moment of the variants, both factors appearing critical for the re-arrangement of the finely tuned PSI:Fld complex. Processes with FNR are also slightly modulated. Despite the displacements observed, the negative end of the dipole moment points towards the surface that contains the FMN, still allowing formation of complexes competent for efficient ET. This agrees with several alternative binding modes in the FNR:Fld interaction. In conclusion, the FMN in Fld not only contributes to the redox process, but also to attain the competent interaction of Fld with FNR and PSI.

1. Introduction

The function of Photosystem I (PSI) in phothosynthesis is to reduce NADP$^+$ to NADPH, that will then be used in CO_2 assimilation. This occurs via reduction of the soluble [2Fe–2S] Ferredoxin (Fd) by PSI, and subsequent reduction of NADP$^+$ by Fd_{rd} is catalysed by Ferredoxin-NADP$^+$ reductase (FNR). In most cyanobacteria and some algae under low iron conditions Flavodoxin (Fld) (a FMN flavoprotein) substitutes for the Fd in this reaction. Thus, two Fld_{sq} molecules transfer two electrons from two PSI molecules to one FNR [1–3]. The role of individual Fld residues on the protein interaction with PSI and FNR has been widely analysed using site-directed mutagenesis [4–7]. These studies have shown that the Fld interactions, particularly with FNR, are less specific than those in other ET complexes, with the bound state being composed of a dynamic ensemble of conformations rather than a single conformation [1,4,8–12]. Experimental and theoretical studies suggest that in Fld the electrostatic alignment appears as one of the major determinants of the orientation of Fld on the partner surfaces and that, once Fld is close enough to its partners, the flavin atoms might be involved in the interaction [4–7,12], and are probably the only ones directly responsible for ET (Figure SP1). In *Anabaena* Fld (*An*Fld) the isoalloxazine 7- and 8-methyl groups are exposed to the solvent, as in most Flds, and present contacts with Asn58, Trp57 and Tyr94 [13]. These residues have been implicated in modulation of the midpoint

Abbreviations: *An*Fld, flavodoxin from *Anabaena*; ApoFld, apoflavodoxin; DDM, β-dodecyl maltoside; ET, electron transfer; ox, oxidised; sq, semiquinone; hq, hydroquinone; $E_{ox/sq}$, midpoint reduction potential for the ox/sq couple; $E_{sq/hq}$, midpoint reduction potential for the sq/hq couple; E_m, midpoint reduction potential for the 2-electron ox/hq reduction; *F*, the Faraday constant; FADS, FAD synthetase; Fld, Fld_{ox}, Fld_{sq}, Fld_{hq}, flavodoxin and in its oxidised, semiquinone and hydroquinone states; FMN_{ox}, FMN_{sq}, FMN_{hq}, FMN and in its oxidised, semiquinone and hydroquinone states; FNR, FNR_{ox}, FNR_{sq}, FNR_{hq}, ferredoxin-NADP$^+$ reductase and in its oxidised, semiquinone and hydroquinone states; K_a, association constant; K_d, dissociation constant; K_r, re-arrangement constant; k_{ap}, apparent observed rate constant; k_{et}, electron transfer rate constant; k_2, second order rate constant; k_{obs}, pseudo-first order observed rate constants; PMS, phenazine methosulfate; PSI, photosystem I; RF, riboflavin; r.m.s.d., root mean square deviation

* Corresponding author. Departamento de Bioquímica y Biología Molecular y Celular, Facultad de Ciencias, Universidad de Zaragoza, 50009-Zaragoza, Spain. Tel.: +34 976762476; fax: +34 976762123.
E-mail address: mmedina@unizar.es (M. Medina).

0005-2728/$ – see front matter © 2009 Elsevier B.V. All rights reserved.
doi:10.1016/j.bbabio.2009.10.012

reduction potentials [14–16], and they modulate the interaction of Fld with PSI and FNR [5,6,17]. We proposed to study the roles played by positions 7 and 8 of the dimethylbenzene ring by replacing FMN in Fld with the high-potential analogues 8-nor-8-Cl-FMN, 7,8-nor-7,8-Cl-FMN, and 7-nor-7-Cl,8-nor-FMN and 7-nor-8-nor-8-Cl-FMN (here in after 8-Cl-FMN, 7,8-diCl-FMN, 7-Cl,8-H-FMN and 7-H,8-Cl-FMN, Figure SP2). These analogues were chosen because they represent substitutions in the positions of the isoalloxazine ring putatively involved in protein interaction and ET, their midpoint-reduction potentials cover a narrow range (-126 mV$>E_m>-152$ mV, Table 1) [18,19] and they have been widely used as mechanistic probes with flavoproteins [20–24]. It was anticipated that the combination of the methyl, hydrogen and chlorine replacements would produce changes that might affect the properties of the Fld surface in the environment of the FMN portion that is exposed to the solvent, and in this way affect the ability of the protein to interact with its partners and to undergo ET.

Replacement of FMN in *An*Fld with these FMN analogues produced strong complexes that stabilise the intermediate semiquinone state of the flavin. Midpoint reduction potentials for the reconstituted Flds have been determined and the ability of these Flds to interact and exchange electrons with PSI and FNR has been analysed. *In silico* structural models of the complexes have been produced. Equilibration of these models by molecular dynamic (MD) simulations required the prior determination of the force field parameters for each FMN_{ox} analogue. The different properties of the new complexes compared to Fld from *An*Fld are discussed on the basis of the properties derived from these structural models, thus providing information about the role played by the solvent-exposed moiety of FMN in complex formation and ET between Fld and PSI or FNR.

2. Materials and methods

2.1. Biological materials

*An*Fld was over-expressed in *Escherichia coli* and purified as described [25]. ApoFld was prepared by treatment with 3% trichloroacetic acid at 4 °C in the presence of dithiothreitol [26]. The precipitated apoprotein was separated from FMN by centrifugation and dissolved in 500 mM MOPS pH 7.0 before dialysis against 50 mM MOPS pH 7.0. *Anabaena* PSI particles were obtained as described [27,28]. The P700 content in PSI samples was calculated from the photoinduced absorbance changes at 820 nm, $\varepsilon = 6.5\ mM^{-1}\ cm^{-1}$ [29]. Chlorophyll concentration was determined according to Arnon [30]. The chlorophyll/P700 ratio of the resulting PSI preparations was 104/1. The same batches of PSI and proteins were used throughout this study.

2.2. Production of FMN analogues

RF analogues 8-nor-Cl-RF, 7,8-nor-7,8-Cl-RF, and 7-nor-7-Cl,8-nor-RF were converted into the corresponding FMN forms using the mutant H28A of FAD synthetase (FADS) from *Corynebacterium ammoniagenes* [31]. Reaction mixtures containing 50 μM of the RF analogue, 0.5 mM ATP, 1 mM $MgCl_2$ and 1.5–3 μM H28A FADS in 50 mM Tris/HCl, pH 8.0, were incubated overnight in the dark at 37 °C. Full conversion of RF into FMN was checked by thin layer chromatography in silica-gel plates [31]. H28A FADS did not accept 7-nor-8-nor-8-Cl-RF as substrate. Therefore, it was converted into FAD using native FADS. Once the reaction was completed, FADS was separated from the flavin by ultrafiltration (Amicon Ultra, Millipore, 10000 MW cut-off). The FAD derivative was hydrolysed to the FMN derivative by incubation with *Naja naja* snake venom (Sigma) for 4 h at room temperature. FMN analogues were purified using a C-18 Sep-Pack Cartridge (Waters). Finally, *Anabaena* ApoFld was incubated with a 1.5-fold molar excess of each FMN analogue in 50 mM MOPS, pH 7.0 for 1 h at 25 °C. Excess flavin was then removed by ultrafiltration and the reconstituted Flds stored at −20 °C.

2.3. Spectroscopic analyses

UV/Vis spectra were recorded in a Kontron Uvikon 942 or in a Cary 300 spectrophotometer, at 25 °C. Fluorescence emission spectra (500–600 nm, with excitation at the ~445 nm/band I maximum of the flavin) were recorded at 25 °C in an Aminco-Bowman Series 2 spectrometer. Circular dichroism spectra were recorded in a Chirascan Applied Photophysics spectropolarimeter in 5 mM MOPS, pH 7.0 at 5 °C, using a 1 mm pathlength cuvette in the far-UV (7 μM Fld) and a 4-mm cuvette in the near-UV and Vis regions (20–30 μM Fld). Unless otherwise stated, all measurements were recorded in 50 mM MOPS, pH 7.0

Dissociation constants (K_d), extinction coefficient changes ($\Delta\varepsilon$) and free energy changes (ΔG) for the complexes between FNR_{ox} and the different Fld_{ox} forms were obtained at 25 °C, by difference absorption spectroscopy as previously described [4,32]. Fitting of the experimental data to the theoretical equation for a 1:1 complex allowed the calculation of K_d and $\Delta\varepsilon$. Errors in the estimated ΔG, K_d and $\Delta\varepsilon$ values were ±15%.

2.4. Determination of midpoint reduction potentials

Midpoint reduction potentials for the ox/sq and sq/hq couples ($E_{ox/sq}$ and $E_{sq/hq}$) of the reconstituted Flds were determined at 25 °C in 50 mM MOPS, pH 7.0 under anaerobic conditions as described [4,16,33]. The cuvette contained 10–35 μM protein, 1 μM redox mediators and, when photoreduction was used, 2 mM EDTA and 1–2 μM deazariboflavin. Stepwise reduction of the protein was achieved by either light irradiation from a 250-W slide projector (in case of *An*Fld) or by stepwise dithionite addition (in case of the FMN analogues). The system was considered to be equilibrated when the potential, measured with a Sycopel Ministat potentiometer, remained stable for at least 20 min, and the UV-Vis spectrum was then recorded. The absorbance spectra allowed to determine

Table 1
Midpoint reduction potentials for the different FMN derivatives both free and bound to ApoFld.

FMN form	E_m (mV)			$E_{ox/sq}$ (mV)			$E_{sq/hq}$ (mV)		
	Free	Fld	$\Delta E_m^{bound\text{-}free}$	Free[a]	Fld	$\Delta E_{ox/sq}^{bound\text{-}free}$	Free[a]	Fld	$\Delta E_{sq/hq}^{bound\text{-}free}$
FMN	−207[b]	−312	−107	−313[b]	−194	119	−101[b]	−431	−331
8-Cl-FMN	−152[c]	−236	−84	−258	−134	124	−46	−337	−288
7,8-diCl-FMN	−126[d]	−156	−30	−232	−89	143	−20	−222	−202
7-H,8-Cl-FMN	−144[c]	−245	−101	−250	−128	122	−38	−362	−324
7-Cl,8-H-FMN	−128[d]	−200	−72	−234	−101	133	−22	−298	−276

E_m data for the free flavins are at pH 7.0. Data for the Flds were obtained in 50 mM MOPS pH 7.0 at 25 °C.
[a] Calculated as indicated in equations [5] and [4] from [46] with the assumption that the semiquinone formation constant (K) for the FMN analogues is the same as that of FMN.
[b] Data from [33, 46].
[c] Data from [48].
[d] Data from [47].

the concentrations of the different redox species at equilibrium in each reduction step [16]. The midpoint potentials for the two redox couples were calculated by linear regression analysis of the plots of potential versus logarithm of the concentration ratio (ox/sq or sq/hq) according to the Nernst equation. The following dyes were used as mediators: anthraquinone-1,5-disulfonate ($E_{m,pH7} = -174$ mV), 1,2-naphthoquinone ($E_{m,pH7} = -143$ mV), and anthraquinone-2-sulfonate ($E_{m,pH7} = -225$ mV) for the determination of $E_{ox/sq}$ and rosinduline ($E_{m,pH7} = -281$ mV), benzylviologen ($E_{m,pH7} = -359$ mV) and methylviologen ($E_{m,pH7} = -446$ mV) for the determination of $E_{sq/hq}$. Error in the $E_{ox/sq}$ and $E_{sq/hq}$ determination was estimated to be ± 5 mV.

2.5. Laser-flash fast kinetics absorption spectroscopy measurements

ET processes between PSI and Fld were studied by laser-flash absorption spectroscopy at 25 °C as described [4,17,34]. Briefly, PSI photoexcitation was achieved by irradiating the sample with a 337 nm laser-flash (PTI PL-2300 nitrogen laser; flash duration, 0.6 ns). Flash-induced absorbance changes were followed by illuminating the sample with a perpendicular monochromatic light beam at the desired wavelength, the signal being detected by a photomultiplier, amplified and recorded in a digital oscilloscope. For the study of the interaction and ET between PSI and Fld_{ox}, the standard reaction mixture contained, in a final volume of 1 ml, 20 mM Tricine/KOH, pH 7.5, 0.03% β-dodecyl maltoside (DDM), an amount of PSI-enriched particles equivalent to 50 μg of chlorophyll ml^{-1}, 50 nM phenazine methosulfate (PMS), 2 mM $MgCl_2$, 2 mM sodium ascorbate, and Fld at varying concentrations. This amount of PMS is enough to reduce PSI in the time between flashes by acting as a high-turnover intermediate between the excess of ascorbate present in the sample and PSI. Fld_{sq} formation was monitored between 565 and 580 nm, depending on the spectra of the Fld variant. Experiments at different $MgCl_2$ concentrations were carried out under the same conditions with a final Fld concentration of 20 μM. For the analysis of the ET from PSI to Fld_{sq}, a mixture containing only the Tricine/KOH buffer, PMS and $MgCl_2$ was degassed by argon bubbling for at least 40 min. DDM, PSI, Fld and sodium ascorbate were subsequently added, together with 10 nM FNR and 0.5 mM NADPH. The reaction mixture was then incubated for 5 min to allow Fld_{sq} formation by the NADPH/FNR system [1,2,35]. After laser irradiation, Fld_{sq} disappearance was followed at 570 nm, an isosbestic point for *Anabaena* PSI oxidation-reduction. Stepwise addition of Fld, to produce the concentration profile dependence, was accompanied with the injection of 50–100 μl of air into the cuvette to avoid the accumulation of Fld_{hq}, followed by a few minutes incubation to ensure generation of Fld_{sq}.

In both type of experiments each kinetic trace was the average of 40–50 measurements, with 30 s time spacing between flashes [36]. For the systems showing monophasic traces, kinetic analyses were carried out according to the two-step reaction mechanisms previously proposed [36,37]. For the systems showing biphasic kinetic traces, k_{on}, k_{off} and K_r minimal values for the additional re-arrangement step in the reaction mechanism were determined according to Sigfridsson et al. [38]. The estimated error in the observed pseudo-first order rate constants (k_{obs}) determination was less than 20%, based on reproducibility and signal-to-noise ratios. Errors in the values estimated for the complex association constant (K_a) and the first-order ET rate constant (k_{et}) were ± 15 and ± 5 %, respectively.

2.6. Stopped-flow kinetic measurements

The reaction between FNR_{hq} (produced by photoreduction with 5-deazariboflavin) and the reconstituted Fld_{ox} variants was analysed in 50 mM MOPS, pH 7.0, at 25 °C under anaerobic conditions using an Applied Photophysics SX17.MV spectrophotometer [17,32]. The proteins were mixed at a ~1:1 molar ratio, with a final concentration of ~10 μM and evolution of the processes was followed in the 400–800 nm range using a photodiode detector. The apparent observed rate constants (k_{ap}) were calculated by fitting the evolution of the semiquinone maxima for each Fld (~570–590 nm) to mono- or bi-exponential processes. Estimated errors in the determined values were $\pm 15\%$.

2.7. Structural models for Flds reconstituted with different FMN analogues

In silico reconstituted Fld models were produced by replacing the FMN_{ox} cofactor in the three-dimensional structure of *An*Fld_{ox} (PDB code: 1FLV) with each of the corresponding FMN analogues. To determine the force field parameters for FMN_{ox} and its different analogues the geometries of their molecular structures (including FMN_{ox}) were optimized using Gaussian 03 with a Hartree–Fock method and 6–31G* basis set [39]. The corresponding molecular electrostatic potentials (MEP) were calculated using the same methodology. The calculated MEP were used to derive the restrained potential charges (RESP) using the RED program [40]. Antechamber programs were used to assign the atom and bond types of the general amber force field and the PARMCHK to add missing parameters [41,42].

MD simulations were performed with AMBER 9.0 [41]. The force field was amber94 with the addition of the parameters derived for the FMN_{ox} analogues. Each molecular system was neutralised by the addition of 17 sodium ions, and solvated with TIP3P water model in an

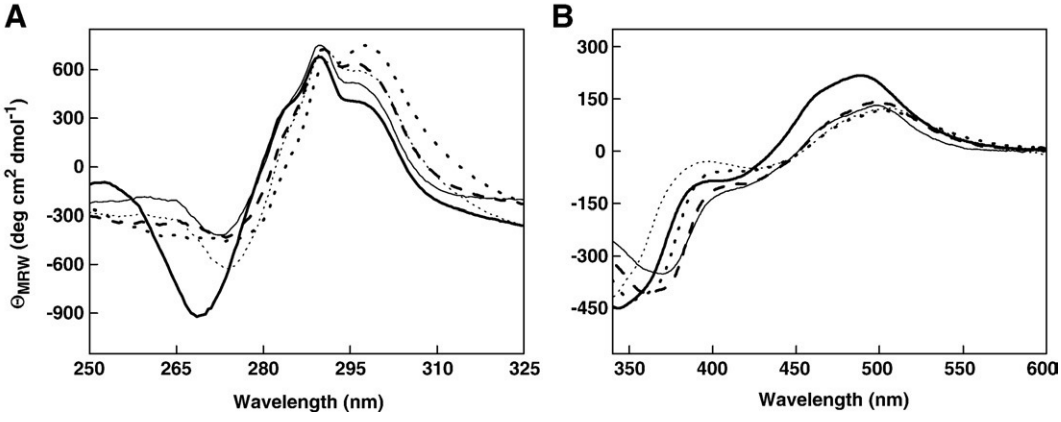

Fig. 1. (A) near-UV and (B) visible CD spectra of *An*Fld (thin solid line), 8-Cl-FMN:Fld (bold dashed line), 7,8-diCl-FMN:Fld (bold dotted line), 7-Cl,8-H-FMN:Fld (thin dotted line) and 7-H, 8-Cl-FMN:Fld (bold solid line) in 5 mM MOPS pH 7.0.

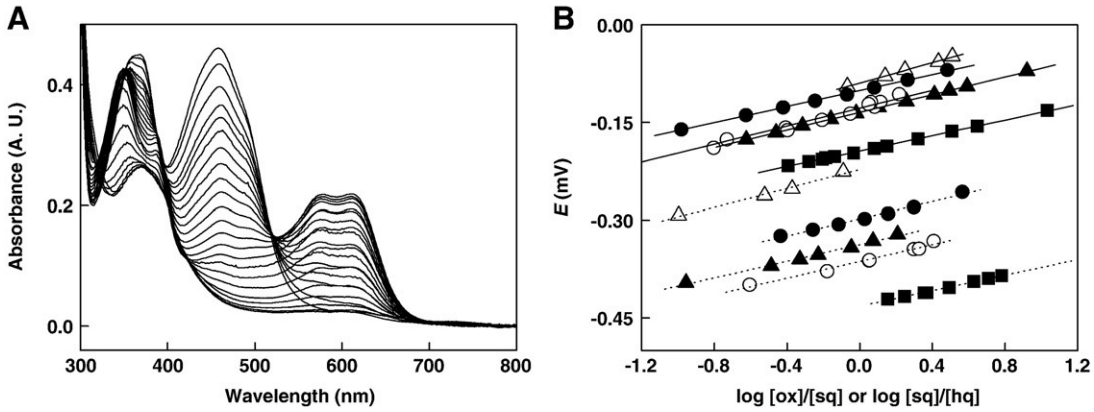

Fig. 2. (A) Absorbance spectra obtained during photoreduction and redox titration of 7-Cl,8-H-FMN:Fld. Changes in the semiquinone band (550-700 nm), band-I (~464 nm) and band-II (~ 373 nm) of the flavin along the reduction process are shown. (B) Nernst plots for ox/sq (solid lines) and sq/hq couples (dotted lines) of the different Fld forms in 50 mM MOPS, pH 7.0 and 25 °C: *An*Fld (■), 8-Cl-FMN:Fld (▲), 7,8-diCl-FMN:Fld (△), 7-H,8-Cl-FMN:Fld (●) and 7-Cl,8-H-FMN:Fld (○).

orthorhombic box. The cut-off distance for the non-bonded interactions was 10 Å. Solvent molecules and counter ions were relaxed and allowed to redistribute around the restrained protein molecule by minimization with 1000 steps of Steepest Descent (SD) and 2000 steps of Conjugate Gradient (CG), the protein atoms were constrained with a harmonic force constant of 500 kcal/mol Å^2. A second energy minimization was carried out with 2000 steps SD and 3000 steps of CG also allowing protein relaxation. The resulting system was heated from 0 K to 300 K at constant volume with the protein atoms constrained with a harmonic force constant of 10 kcal/mol Å^2. The system was then equilibrated during 100 ps at 300 K, using a Langevine temperature equilibration algorithm, and 1 atm, with periodic boundary conditions, and using the Particle Mesh Ewald method to treat long-range electrostatic interactions. Production runs consisted of 8–10 ns of MD with 2 fs steps. Temperature was kept at 300 K using a Berendsen constant temperature algorithm and the pressure at 1 atm using a weak-coupling pressure algorithm. System coordinates were collected every 2 ps. During equilibration and simulations the leapfrog Verlet integration scheme and the SHAKE algorithm were used.

Three-dimensional structures and trajectories were visually inspected using the programs PyMOL and VMD [43,44]. Interatomic distances

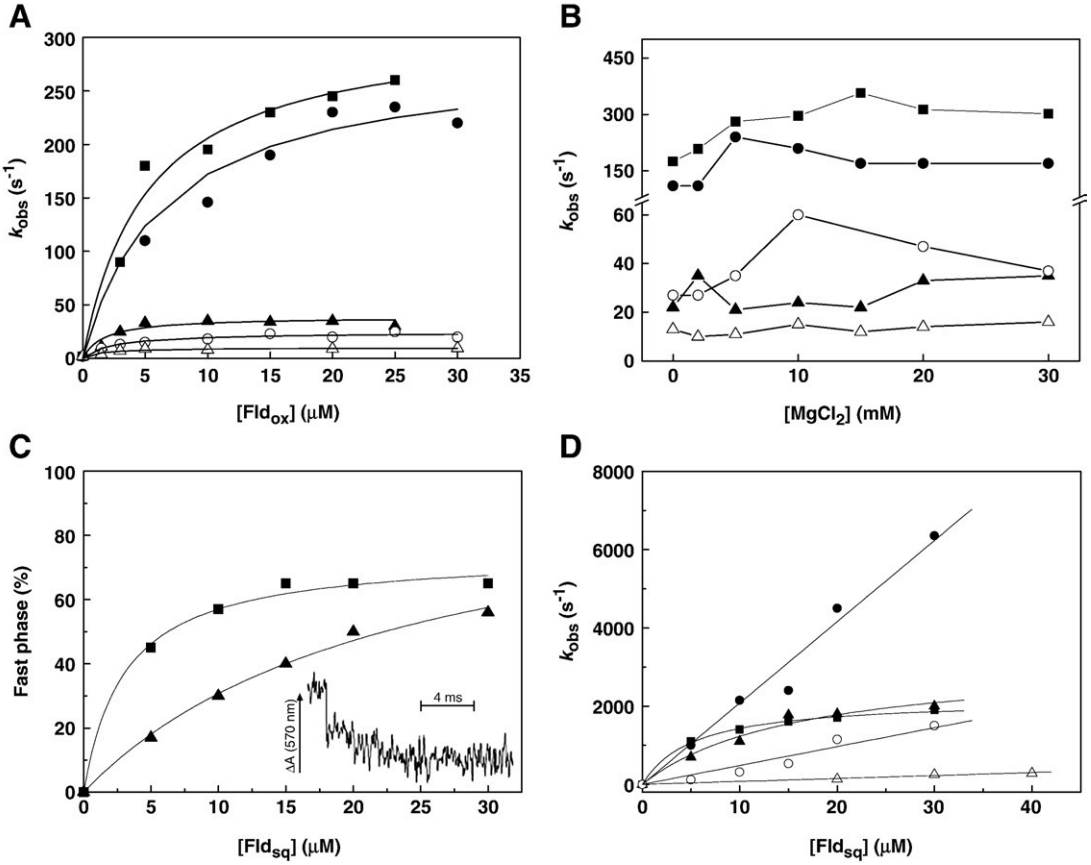

Fig. 3. Reduction of the different Fld$_{ox}$ and Fld$_{sq}$ variants by PSI. (A) Dependence on Fld concentration of the k_{obs} for the reduction of Fld$_{ox}$. (B) Effect of $MgCl_2$ on k_{obs} for the reduction of Fld$_{ox}$. (C) Dependence on Fld concentration of the percentage of fast phase, with respect to the total signal amplitude, for the reduction of Fld$_{sq}$. The inset shows the kinetics for the reduction of 8-Cl-FMN:Fld at 15 μM Fld. (D) Dependence on Fld concentration of the k_{obs} for the slow phase for Fld$_{sq}$ reduction (*An*Fld and 8-Cl-FMN:Fld) or the single observed phase (rest of Fld variants). *An*Fld (■), 8-Cl-FMN:Fld (▲), 7,8-diCl-FMN:Fld (△), 7-H,8-Cl-FMN:Fld (●), and 7-Cl,8-H-FMN:Fld (○).

Table 2
Kinetic parameters for the reduction of Fld_{ox} and Fld_{sq} forms by PSI.

Fld form	Reduction of Fld_{ox}		Reduction of Fld_{sq}			
	K_a (M^{-1})	k_{et} (s^{-1})	K_a (M^{-1})	k_{et} (s^{-1})	K_r	k_2[a] (M^{-1} s^{-1})
*An*Fld	3.0×10^5[b]	315[b]	2.1×10^5	>50000	2.9	
8-Cl-FMN:Fld	4.5×10^5	38	1.6×10^5	>50000	4.0	
7,8-diCl-FMN:Fld	6.3×10^5	10				7.5×10^6
7-H,8-Cl-FMN:Fld	1.1×10^5	313				2.0×10^8
7-Cl,8-H-FMN:Fld	3.7×10^5	24				4.8×10^7

[a] A linear dependence was observed and only the second-order rate constant could be determined.
[b] *An*Fld data were again determined in the present study obtaining similar values to those previously reported [17].

and angles, as well as the root mean square deviation (r.m.s.d.) from a given structure, were monitored using PTRAJ [41]. Accessible surface area (ASA) was estimated with NACCESS (http://www.bioinf.manchester.ac.uk/naccess). The van der Waals radii of analogues used for determining the ASA were the same as in the MD, and a spherical probe with a radius of 1.5 Å was used.

3. Results

3.1. Spectral properties of the Flds reconstituted with FMN analogues

The far-UV CD spectra of Flds reconstituted with different FMN analogues indicate no major structural perturbations in the protein folding. However, position and relative intensities of minima, maxima and shoulders varied in the near-UV and Vis for 7-H,8-Cl-FMN:Fld, 7-Cl,8-H-FMN:Fld and 7,8-diCl-FMN:Fld (Fig. 1). These data suggest changes in the environment of protein aromatic residues, as well as in the flavin isoalloxazine ring environment. The general shape of the Vis absorbance spectra of reconstituted Flds is similar to that of *An*Fld, but differences occur in the position of maxima, their extinction coefficients and the relative intensities of their respective two flavin bands, reflecting the differences also observed for the free FMN analogues (Figure SP2, Table SP1). Upon interaction with ApoFld, the flavin bands of the free FMN analogues are red-shifted (band I by 12–18 nm; band II by 1–4 nm) (Figure SP2, Table SP1). All the Fld variants stabilised the blue neutral semiquinone (Fig. 2A). The shape and the positions of their semiquinone long-wavelength band absorbance maxima, as well as the isosbestic points for their ox/sq transitions, are generally different from those of *An*Fld_{sq} (Table SP1). 8-Cl-FMN:Fld_{sq}, 7,8-diCl-FMN:Fld_{sq} and 7-Cl,8-H-FMN:Fld_{sq} showed two maxima in the neutral semiquinone band, which are red-shifted compared to the single absortium maximum for *An*Fld_{sq}. The ox/sq isosbestic point for 7-Cl,8-H-FMN:Fld is also red-shifted. 7-H,8-Cl-FMN:Fld_{sq} had a single maximum that was blue-shifted, as was the isosbestic point. The extinction coefficient for these Fld_{sq} variants was in general smaller than that of *An*Fld_{sq} (Table SP1). The maximum extent of semiquinone stabilisation for 8-Cl-FMN:Fld, 7-H,8-Cl-FMN:Fld and 7-Cl,8-H-FMN:Fld was similar to that of *An*Fld (~97%), while it decreased for 7,8-diCl-FMN:Fld (~70%). Finally, the flavin fluorescence quenching levels observed when ApoFld interacted with the FMN analogues are slightly lower than reported for FMN, with 7,8-diCl-FMN:Fld and 7-H,8-Cl-FMN:Fld still showing ~9 % of the free flavin emission intensity (<3% for FMN in Fld) [15].

3.2. Midpoint reduction potentials of the Fld variants

The E_m, $E_{ox/sq}$ and $E_{sq/hq}$ of the free FMN analogues used in this work and modified at positions 7 and 8 were 55–80 mV less negative than those of free FMN (Table 1) [45–48]. Similarly, E_m, $E_{ox/sq}$ and $E_{sq/hq}$ of their reconstituted Flds were less negative than those of *An*Fld, being the changes larger in $E_{sq/hq}$ (70–210 mV less negative) than in $E_{ox/sq}$ (60–105 mV less negative) (Table 1, Fig. 2). As observed for FMN, the binding of the FMN analogues to ApoFld shifted their $E_{ox/sq}$ to less negative values and the $E_{sq/hq}$ to more negative ones, and stabilised the flavin semiquinone (Table 1). This shift in $E_{ox/sq}$ was in general slightly larger for the FMN analogues ($\Delta E^{bound\text{-}free}$ from +122 to +143 mV) than for FMN ($\Delta E^{bound\text{-}free} = +119$ mV), while the shift in $E_{sq/hq}$ was smaller ($\Delta E^{bound\text{-}free}$ from −202 to −324 mV *versus* $\Delta E^{bound\text{-}free} = -331$ mV) (Table 1). 8-Cl-FMN and, especially, 7-H,8-Cl-FMN showed the $\Delta E^{bound\text{-}free}$ values most similar to FMN, while 7-Cl,8-H-FMN and, in particular, 7,8-diCl-FMN, showed considerably smaller values (Table 1).

3.3 Pre-steady-state kinetic analysis of the reduction of Fld_{ox} and Fld_{sq} variants by PSI

Although the Fld_{sq}/Fld_{hq} couple is the one thought to be involved in ET from PSI to FNR, a physiological role for the Fld_{ox}/Fld_{sq} one cannot be ruled out [4,10,35]. Therefore, one-electron reduction of both Fld_{ox} and Fld_{sq} by PSI has been analysed for the Fld variants using laser-flash absorption spectroscopy. The electron reduction of all Fld_{ox} variants by PSI showed a monoexponential kinetic trace, as observed for *An*Fld [34]. However, reduction of 8-Cl-FMN:Fld_{ox}, 7-Cl,8-H-FMN:Fld_{ox} and, particularly, 7,8-diCl-FMN:Fld_{ox} became highly impaired (Fig. 3A). The nonlinear dependences of the k_{obs} on Fld_{ox} concentration suggest that a transient PSI:Fld_{ox} complex is formed prior to ET in these reactions, as reported for *An*Fld. Minimal values for both the K_a for the PSI:Fld_{ox} complex formation and the k_{et} can be determined (Fig. 3A and Table 2) [7,34]. Replacement of the FMN methyl groups hardly affected K_a, but, with the exception of 7-H,8-Cl-FMN:Fld, all the Fld_{ox} variants were much poorer electron acceptors from PSI (Table 2). A re-arrangement of the initial PSI:Fld_{ox} interaction complex to achieve optimal ET is reflected for *An*Fld on the biphasic dependence of k_{obs} with $MgCl_2$ concentration (Fig. 3B) [34,36]. This

Table 3
Interaction parameters obtained by differential spectroscopy and kinetic parameters from stopped-flow analysis for the processes of FNR with the different Fld variants.

Fld_{ox} form	Parameters for the FNR_{ox}:Fld_{ox} interaction					Fast kinetic parameters for the reduction of Fld_{ox} by FNR_{hq}	
	K_d (μM)	$\Delta\varepsilon_{band\ I}$ (mM^{-1} cm^{-1})	Band II (nm)	Band I (nm)	ΔG_{ox}[a] (kcal mol^{-1})	k_{ap1} (s^{-1})	k_{ap2} (s^{-1})
*An*Fld	0.65	2.7	392	466	−8.4	1.6	0.3
8-Cl-FMN:Fld	0.55	2.9	393	464	−8.5	100	20
7,8-diCl-FMN:Fld	0.55	2.8	396	465	−8.5	220	30
7-H,8-Cl-FMN:Fld	0.63	2.2	395	464	−8.5	18	2.0
7-Cl,8-H-FMN:Fld	0.88	2.5	397	465	−8.3	100	25

Data obtained in 50 mM MOPS pH 7.0 at 25 °C.
[a] Calculated according to the $\Delta G_{ox} = -RT \ln 1/K_d$.

bell-shaped profile is also observed for 7-H,8-Cl-FMN:Fld, and 7-Cl,8-H-FMN:Fld (Fig. 3B), but the k_{obs} maxima are shifted to slightly lower salt concentrations (about 5–10 mM). For 8-Cl-FMN:Fld and 7,8-di-Cl-FMN:Fld, the lack of effect of $MgCl_2$ on k_{obs} correlates with the low ET rates observed at all salt concentrations.

Reduction of $An\text{Fld}_{sq}$ and 8-Cl-FMN:Fld_{sq} by PSI showed biphasic kinetic traces, with a first fast phase, whose amplitude increases with protein concentration up to reach a maximum value (Fig. 3C), and a subsequent slower phase with k_{obs} values depending on the Fld concentration and following a saturation profile (Fig. 3D). Biphasic kinetics have been previously reported for similar systems from other cyanobacteria [35,49] (and see below). This kinetic behaviour conforms to a model in which the initial complex, whose formation is characterised by a K_a, undergoes a reorganization step to an optimal configuration, described by a re-arrangement constant, K_r, for the ET to take place [38]:

$$\text{Fld}_{sq} + \text{PSI}_{red} \overset{K_a}{\leftrightarrows} (\text{Fld}_{sq}\text{: PSI}_{red}) \underset{k_{off}}{\overset{k_{on}}{\leftrightarrows}} (\text{Fld}_{sq}\text{: PSI}_{red})^* \overset{k_{et}}{\rightarrow} \text{Fld}_{hq} + \text{PSI}_{ox}$$

$$\text{where } K_r = k_{on} / k_{off}$$

According to this model, the k_{et} value can be obtained directly from the k_{obs} for the fast phase. However, in our case this fast phase mainly occurred within the dead time of the instrument (50 μs), indicating a minimal k_{et} value of about 50000 s^{-1}, which is in the order of those described for other cyanobacterial systems [35,49]. Values for K_a and k_{on} can be estimated from the extrapolation of k_{obs} for the slow phase to infinite Fld concentration (Fig. 3D) [37,38]. Thus, the values obtained for k_{on} (2200 s^{-1} and 2800 s^{-1} for $An\text{Fld}_{sq}$ and 8-Cl-FMN:Fld_{sq}, respectively) and K_a (Table 2) were similar for both Fld variants. Moreover, from the extrapolation of the percentage of fast phase -with regard to the total signal amplitude- to infinite acceptor concentration (Fig. 3C) and the values of k_{on} previously determined, an estimation of k_{off} (750 s^{-1} and 700 s^{-1} for $An\text{Fld}_{sq}$ and 8-Cl-FMN:Fld_{sq}, respectively), and then also for K_r (Table 2), can be obtained [38]. Again, similar values for all these kinetic constants were calculated for both variants (Table 2). In contrast to *An*Fld, the PSI-mediated reduction of 7-H,8-Cl-FMN:Fld_{sq}, 7-Cl,8-H-FMN:Fld_{sq} and 7,8-diCl-FMN:Fld_{sq} result in monoexponential kinetic behaviour, where k_{obs} is linearly dependent on the Fld_{sq} concentration (Fig. 3D), as previously reported for the slower phase in other PSI systems when interacting with *An*Fld [35,49]. These data suggest that for these Fld variants, ET from PSI to Fld_{sq} occurs by a collisional-type mechanism, without formation of a kinetically-detectable complex, and is characterised by a second-order rate constant, k_2 (Table 2) [4,7]. It is interesting to compare the kinetic behaviour of the $An\text{Fld}_{sq}$ reported here for the slower phase (i.e., the interaction step), with that previously shown for other cyanobacterial systems [35,49]. Thus, whereas the different nature of the two constants (K_a here vs. k_2 in [35,49]) precludes a direct comparison, the k_{obs} values are of similar magnitude. Interestingly, the k_2 value here obtained for the 7-H,8-Cl-FMN:Fld_{sq} is similar to the k_2 values for the slower phase previously reported for the systems of *Synechocystis* and *Synechococcus*, thereby suggesting a fine tuning in the optimal transient complex that is easily affected by minor changes at the protein interacting surfaces.

3.4. The interaction of the Fld_{ox} variants with FNR_{ox}

The Fld_{ox}:FNR_{ox} difference spectrum obtained for the different Fld variants showed similar perturbations to those reported for the *An*Fld complex, with only minor shifts in the positions of the flavin band maxima (Table 3) [17,32]. Additionally, the magnitude of difference spectra formed upon FNR_{ox} titration with the different reconstituted Fld_{ox}s reached saturation, allowing determination of K_d and ΔG (Table 3). All the Fld_{ox} variants exhibited values for complex formation with FNR_{ox} very similar to those of *An*Fld. This suggests that replacement of the FMN methyl groups on Fld does not affect binding to the FNR flavin environment.

3.5. Pre-steady-state kinetic analysis of the ET processes from FNR_{hq} to the Fld variants

The reaction of FNR_{hq} with $An\text{Fld}_{ox}$ has been shown as a relatively slow two-step process due to initial production of Fld_{sq} and FNR_{sq}, followed by the reduction of a second Fld_{ox} molecule by the FNR_{sq} produced in the first step [6,17,32]. A similar behaviour is observed for

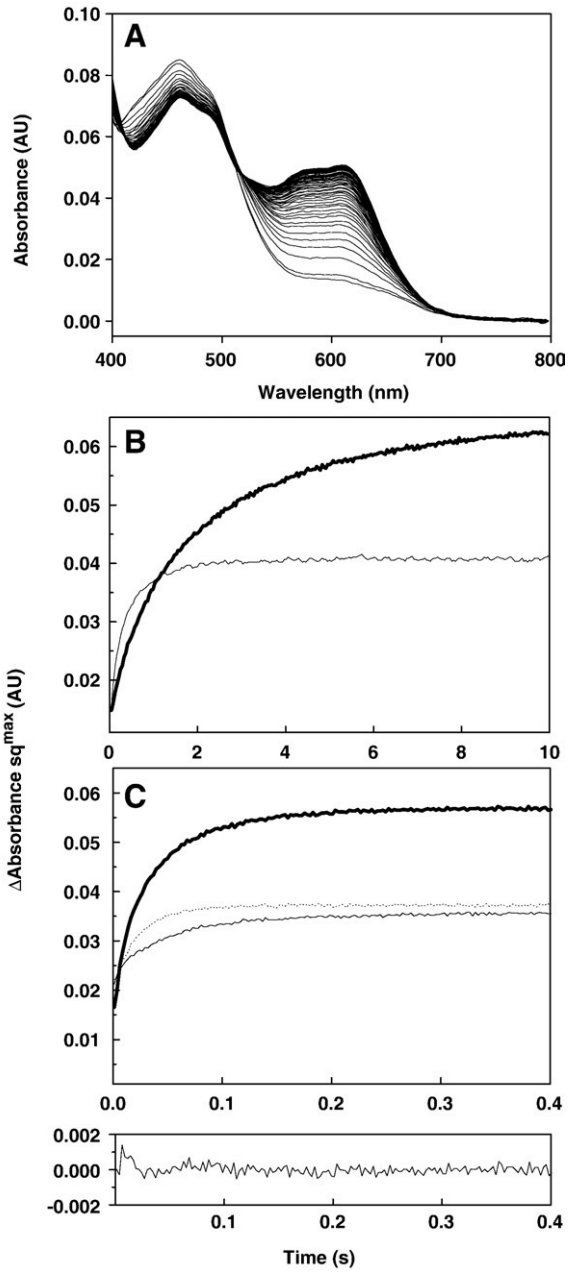

Fig. 4. Stopped-flow kinetic analysis of the anaerobic reduction of the different Fld variants by FNR_{hq}. (A) Evolution of the spectral changes accompanying the reduction of 8Cl-FMN:Fld_{ox} by FNR_{hq}. Spectra shown in the 0–0.18 s range after mixing. Kinetic traces at the maximum wavelength of the semiquinone for each Fld variant are also shown in (B) for the reduction of *An*Fld (bold line) and 7-H,8-Cl-FMN:Fld (thin line) and in (C) for the reduction of 8-Cl-FMN:Fld (bold solid line), 7,8-diCl-FMN:Fld (thin solid line) and 7-Cl,8-H-FMN:Fld (dotted line). The residual for the fitting of the reaction with 8-Cl-FMN:Fld is shown. In all cases FNR and Fld concentrations were 10 μM.

the reduction of the reconstituted Flds with FMN analogues, the kinetic traces in the 600 nm semiquinone region also fitting a biphasic process (Fig. 4). The amplitudes of the kinetic traces are in general similar to or within a factor of 1.5 (larger for most of the variants) of those observed for the reaction with *An*Fld$_{ox}$, the amplitude for the second process being within 2-fold (usually larger) that of the first one. Compared with *An*Fld, the Fld$_{ox}$s reconstituted with the FMN analogues are better electron acceptors from both FNR$_{hq}$ and FNR$_{sq}$ (Table 3). Such behaviour is particularly clear for 8-Cl-FMN:Fld, 7-Cl-,8-H-FMN:Fld and 7,8-diCl-FMN:Fld and is in agreement with the more positive midpoint potentials of these Fld variants. The physiological ET from Fld$_{hq}$ to FNR was not analysed, since the $E_{sq/hq}$ values for these Fld variants suggest that very little reduction of FNR will occur.

3.6. Three-dimensional models for reconstituted Flds

Replacement of the 8-methyl group by chlorine produces an increase in the negative character of the C(8) and a decrease of the negative charge density on the pyrazine and pyrimidine rings (Fig. 5). Such effects are greater when the 7- and 8-methyl groups are simultaneously replaced, either one with a Cl and the other one with an H, but more especially, if both of them are simultaneously replaced with Cl. Therefore, as expected, the substituents introduced at positions 7- and 8- of FMN$_{ox}$ have an electron withdrawal effect on the pyrazine and pyrimidine rings.

To validate the method used for the production of 3D models for the complexes of these FMN$_{ox}$ analogues with *Anabaena* ApoFld, *An*Fld was treated in the same way. Using the calculated parameters for free FMN$_{ox}$, the *An*Fld$_{ox}$ model provided a structure that after MD simulation gave a r.m.s.d. backbone of 1.3 Å with regard to the crystallographic structure of *An*Fld$_{ox}$ [13]. The r.m.s.d. value was under 1.4 Å when comparing the models of Fld reconstituted with FMN analogues and the model of Fld reconstituted with FMN. Slightly different relative orientations were observed between the benzene ring of the isoalloxazine and the side chain of Trp57 along the MD for the different variants. However, the orientation of Tyr94 compared to the flavin ring and the distance and orientation of the putative H-bond between Ile59NH and the N(5) positions of FMN$_{ox}$ are the same as in *An*Fld (not shown) [13]. As a consequence of the modifications introduced in the free FMN$_{ox}$, minor differences in the solvent accessibility of the benzene moiety of the flavin ring are observed (Table SP2), and solvent accessibility is only substantially increased for C(7) and C(8) when the substituent at each position is a proton.

4. Discussion

Changes at the FMN benzenoid methyl groups do not prevent the corresponding Fld$_{ox}$s from accepting electrons from PSI, FNR$_{hq}$ or FNR$_{sq}$ following transient complex formation, and they have only little effect on the strength of the PSI:Fld$_{ox}$ and FNR$_{ox}$:Fld$_{ox}$ interactions (Fig. 3A and B, Tables 2 and 3).

However, only 7-H,8-Cl-FMN:Fld$_{ox}$ retains the k_{et} in accepting electrons from PSI (Fig. 3A), and a poor and reverse correlation is observed between these k_{et} values and $E_{ox/sq}$ (Fig. 7A), but do maintain similar K_a values. Thus, subtle changes in the cofactor area of Fld severely affect the ET step whereas the interaction affinity remains unaffected, indicating again the fine tuning in the productive ET complex. Reduction of *An*Fld$_{sq}$ by PSI, described here for the first time, shows the biphasic kinetics previously observed in the corresponding *Synechocystis* and *Synechococcus* systems [35], but it differs from the others in a major way in that the slow phase becomes saturated at high protein concentration (Table 2, Fig. 3C and D). None of the Fld variants, except 8-Cl-FMN:Fld, exhibit the characteristic biphasic kinetic behaviour of *An*Fld. However, the linear dependence of k_{obs} on protein concentration observed for the variants 7-H,8-Cl-FMN:Fld$_{sq}$, 7-Cl,8-H-FMN:Fld$_{sq}$ and 7,8-diCl-FMN:Fld$_{sq}$ suggests that the modifications in the cofactor alter the bimolecular interaction step. In fact, the complex formed between PSI and Fld seems to be somewhat delicate and in other cyanobacteria linear dependencies have been observed [35,50]. While the values for k_{obs} and k_2 for 7-H,8-Cl-FMN:

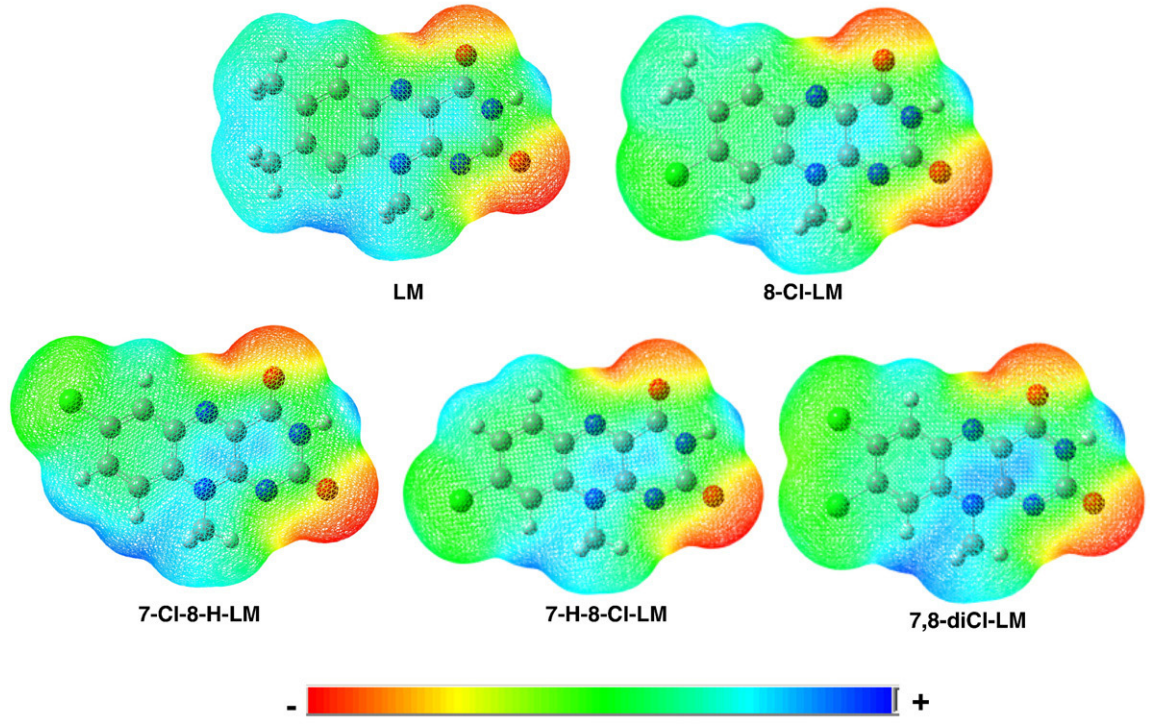

Fig. 5. Electrostatic surface potential distribution within the different lumiflavin (LM) analogues in the oxidised state. MEP were calculated using a Hartree–Fock method and 6-31G* basis set.

Fld_{sq} are similar to those observed in the equivalent *Synechocystis* and *Synechococcus* Fld, the values for 7-Cl,8-H-FMN:Fld_{sq} and 7,8-diCl-FMN:Fld_{sq} show that a drastic decrease in reactivity has occurred, although the driving force of the ET reaction for these variants has actually increased (Table 1). The k_{obs} values for 7-H,8-Cl-FMN:Fld_{sq} are considerably greater than those of *An*Fld at similar protein concentrations. This could be due to the enhancement in the driving force of the reaction, but might also indicate that the native complex is not optimised for ET [4]. Notable is the opposite behaviour of 8-Cl-FMN:Fld in its oxidised and semiquinone forms when reduced by PSI (Fig. 3): whereas the semiquinone efficiently reacts with PSI, and is the only variant that maintains the biphasic behaviour of *An*Fld, the oxidised species shows a greatly diminished reactivity. All of these data indicate that the methyl groups of FMN, as well as the cofactor redox state, contribute to the re-orientation of Fld in the PSI docking site.

The Fld_{ox} variants are more rapidly reduced by both FNR_{hq} and FNR_{sq} than *An*Fld_{ox} (Table 3, Fig. 4), in agreement with the increase in the reaction driving force expected from their less negative $E_{ox/sq}$ values (Table 1). Nevertheless, although a positive correlation exists between the rate constants for those processes and $E_{ox/sq}$, some of the points diverge from the correlation, in particular 7-H,8-Cl-FMN:Fld_{ox} (Fig. 7B). This observation suggests that the ET competent complex produced between FNR and 7-H,8-Cl-FMN:Fld_{ox} is less optimized for ET than that with *An*Fld_{ox}, while interactions with other variants, as 7,8-diCl-FMN:Fld_{ox}, might be more optimized than *An*Fld. Therefore, although the driving force of the reaction contributes greatly to the faster ET processes, the characteristics of the groups at the 7- and 8-positions of FMN must in someway modulate the competent ET orientation of Fld on the FNR.

The models produced for these Fld_{ox} variants show a certain surface flexibility, including the FMN environment, as expected for a globular protein. Therefore, Fld will not behave as a rigid body in the interaction with its partners. Previous studies suggest that in the Fld:FNR system interactions do not rely on a precise complementary surface of the reacting molecules and several ensembles might be competent for ET [4]. Therefore, it is not probable that the functional divergences observed here between these variants will arise only from changes in the shape of their surface. Similarly, the MEP surfaces calculated for the different Fld_{ox}s structural models at different points along the equilibrium of the MD simulation show only minor divergences (Fig. 6A). In all cases the Fld interaction surface that contains the FMN shows a strong negative potential, apparently only slightly increased in 8-Cl-FMN:Fld_{ox}. However, changes in the averaged magnitude of the molecular dipole moment can be predicted between the variants (Fig. 6A and B) and, correlations between the rate constants and the averaged magnitude of the molecular dipole moment follow similar patterns to those discussed above for $E_{ox/sq}$ (Fig. 7). This indicates that the magnitude of the molecular dipole moment contributes to the re-arrangements required for a reaction-competent interaction. The dispersion of the experimental points from the correlation fittings, and particularly the negative correlations observed with PSI, suggests that other factors apart from the midpoint reduction potentials and the magnitude of the molecular dipole moment contribute to the observed effects. The initial orientation driven by the alignment of dipole moment of the Fld molecule with that of the partner has also been reported as a critical factor in this system [4]. Fig. 6C shows the spatial distribution along the MD equilibrium of the molecular dipole moment for the different reconstituted Fld_{ox}s. Considerable shifts in the orientation of the

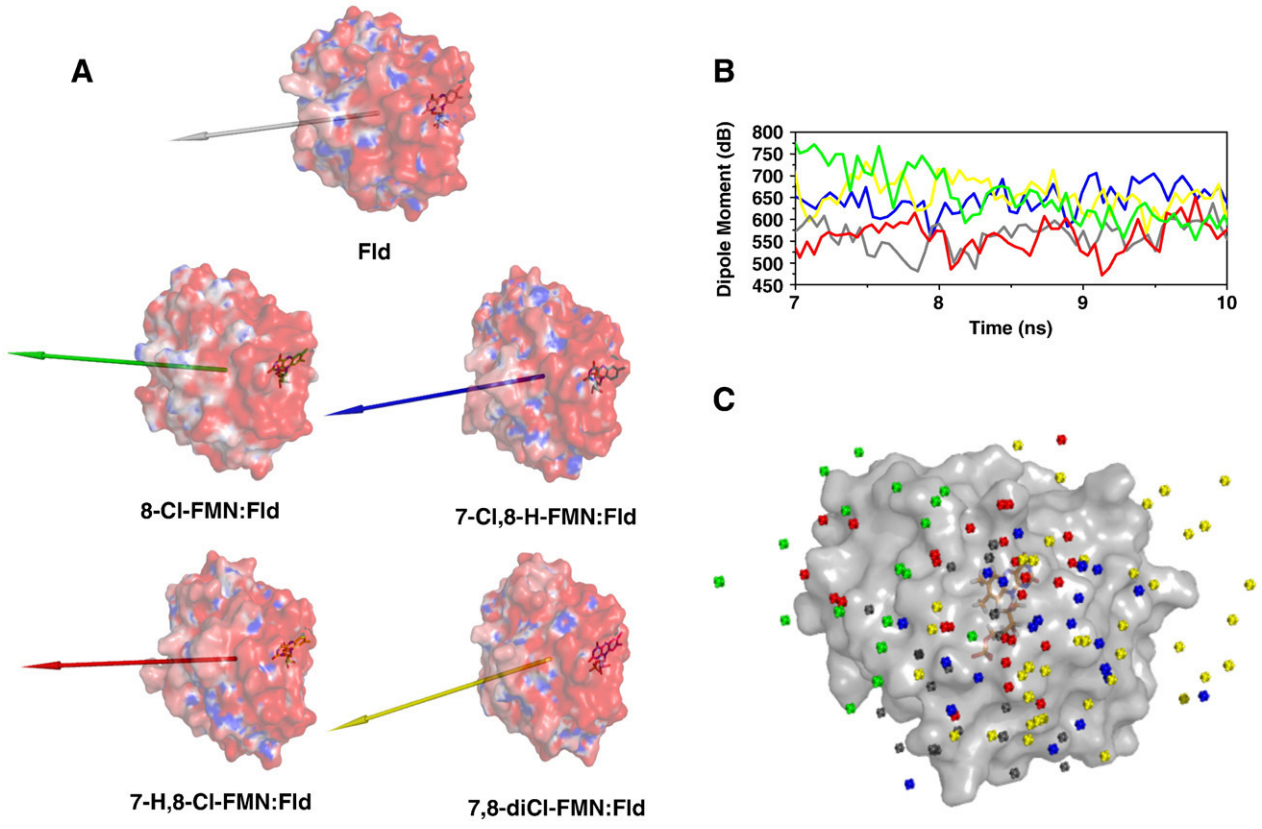

Fig. 6. (A) Molecular surfaces with electrostatic potentials for one of the equilibrium MD structures of the different Fld variants. The FMN group is shown in sticks and CPK coloured. The relative magnitude and orientation of the dipole moments of the corresponding structures are shown by arrows. (B) Time evolution of the molecular dipole moment magnitude along the MD equilibrium for the different Fld variants. (C) Spatial distribution of the molecular dipole moment direction along the MD equilibrium for the different Fld variants with regard to the protein surface. Code colour for the molecular dipole moments; *An*Fld in grey, 8-Cl-FMN:Fld in green, 7-Cl,8-H-FMN:Fld in blue, 7-H,8-Cl-FMN:Fld in red and 7,8-diCl-FMN:Fld in yellow.

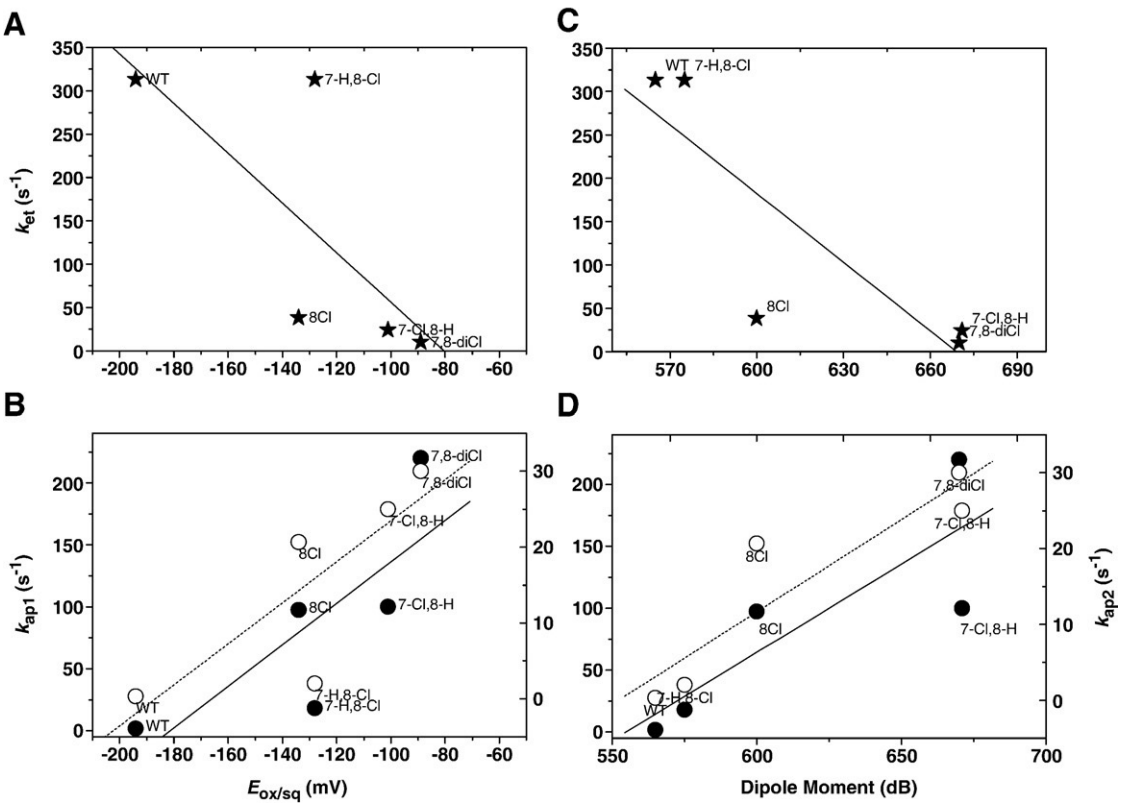

Fig. 7. Correlation of the rates of reduction of the Fld_{ox} variants reconstituted with high-potential FMN analogues with $E_{ox/sq}$ values and with the averaged magnitude of the molecular dipole moment at the MD equilibrium. (A) k_{et} for the reduction by PSI with $E_{ox/sq}$. (B) k_{ap1} (●) and k_{ap2} (○) for the reduction by FNR with $E_{ox/sq}$. (C) k_{et} for the reduction by PSI with averaged dipole moment. (D) k_{ap1} (●) and k_{ap2} (○) for the reduction by FNR with averaged dipole moment. Linear fittings of the data are shown. In C and D, solid and dashed thin lines correspond to k_{ap1} and k_{ap2}, respectively.

molecular dipole moment appear to be produced for 8-Cl-FMN:Fld and 7,8-diCl-FMN:Fld, while smaller deviations are predicted for 7-Cl,8-H-FMN:Fld and 7-H,8-Cl-FMN:Fld. These shifts produced displacements in the orientation of the negative end of the dipole moment associated with the flavin ring, and, therefore, in the docking orientations between these Flds and FNR or PSI. As mentioned above, the effect in the change of the dipole moment orientation appears much more critical in the processes with PSI than in those with FNR. This agrees with the proposal of alternative productive binding modes between FNR and Fld [1,4], while production of the ET competent PSI-FMN:Fld interactions appears to be much more sensitive to subtle changes in the orientation [35]. It has been suggested that linear electron transport between PSI and FNR might occur through a ternary PSI:Fd:FNR or PSI:Fld:FNR complex. However, no direct interaction between PSI and FNR could be demonstrated *in vivo* [50], and our data indicate that the same surface of Fld around its FMN cofactor has to interact with both PSI and FNR, and both contacts cannot occur simultaneously. Therefore, the architecture of such putative interaction remains unknown.

Finally, the study of the role of the substituents at positions 7 and 8 of the isoalloxazine is also of mechanistic interest because of the putative role of these positions as gates for the electrons entering and leaving the flavin ring. In this context, changes in the ASA of the benzene ring position might contribute to changes in reactivity. The changes are small for the variants produced (Table SP2), and only when a proton substitutes for either the 7- or 8-methyls is a considerable increase in the C(7) and C(8) ASA observed. Taking into account that 7-H,8-Cl-FMN:Fld and 7-Cl,8-H-FMN:Fld are the variants that show the greater divergence from the correlations of Fig. 7, changes in ASA might be affecting the reactivity. However, since all variants are able to accept electrons from FNR, these methyls are not critical for the ET process.

In conclusion, subtle changes in the isoalloxazine structure influence the Fld binding abilities and modulate the ET processes by producing different orientations on the surfaces of the partners. This strongly suggests that the FMN group, in addition to its participation in the ET process, contributes to the interaction of Fld with different structural partners and particularly to the re-arrangement of the initial PSI-FMN:Fld interaction.

Acknowledgements

This work has been supported by Ministerio de Educación y Ciencia, Spain (Grant BIO2007-65890-C02-01 to M.M) and by CONSI+D, DGA (Grant PM062/2007 to M.M.). We thank Dr. J.R. Peregrina for production of the programs used to determine molecular dipole moments.

Appendix A. Supplementary data

Supplementary data associated with this article can be found, in the online version, at doi:10.1016/j.bbabio.2009.10.012.

References

[1] M. Medina, Structural and mechanistic aspects of flavoproteins: Photosynthetic electron transfer from photosystem I to $NADP^+$, FEBS J. 276 (2009) 3942–3958.
[2] M. Medina, C. Gomez-Moreno, Interaction of ferredoxin-$NADP^+$ reductase with its substrates: Optimal interaction for efficient electron transfer, Photosynth. Res. 79 (2004) 113–131.
[3] J. Sancho, M. Medina, C. Gomez-Moreno, Arginyl groups involved in the binding of *Anabaena* ferredoxin-$NADP^+$ reductase to $NADP^+$ and to ferredoxin, Eur. J. Biochem. 187 (1990) 39–48.
[4] G. Goñi, B. Herguedas, M. Hervas, J.R. Peregrina, M.A. De la Rosa, C. Gomez-Moreno, J.A. Navarro, J.A. Hermoso, M. Martinez-Julvez, M. Medina, Flavodoxin: a compromise between efficiency and versatility in the electron transfer from

Photosystem I to Ferredoxin-NADP$^+$ reductase, Biochim. Biophys. Acta 1787 (2009) 144–154.
[5] G. Goñi, A. Serrano, S. Frago, M. Hervas, J.R. Peregrina, M.A. De la Rosa, C. Gomez-Moreno, J.A. Navarro, M. Medina, Flavodoxin-mediated electron transfer from photosystem I to ferredoxin-NADP$^+$ reductase in *Anabaena*: role of flavodoxin hydrophobic residues in protein-protein interactions, Biochemistry 47 (2008) 1207–1217.
[6] I. Nogues, M. Hervas, J.R. Peregrina, J.A. Navarro, M.A. de la Rosa, C. Gomez-Moreno, M. Medina, *Anabaena* flavodoxin as an electron carrier from photosystem I to ferredoxin-NADP$^+$ reductase. Role of flavodoxin residues in protein–protein interaction and electron transfer, Biochemistry 44 (2005) 97–104.
[7] I. Nogues, M. Martinez-Julvez, J.A. Navarro, M. Hervas, L. Armenteros, M.A. de la Rosa, T.B. Brodie, J.K. Hurley, G. Tollin, C. Gomez-Moreno, M. Medina, Role of hydrophobic interactions in the flavodoxin mediated electron transfer from photosystem I to ferredoxin-NADP$^+$ reductase in *Anabaena* PCC 7119, Biochemistry 42 (2003) 2036–2045.
[8] J.A. Worrall, W. Reinle, R. Bernhardt, M. Ubbink, Transient protein interactions studied by NMR spectroscopy: the case of cytochrome *c* and adrenodoxin, Biochemistry 42 (2003) 7068–7076.
[9] P.B. Crowley, M.A. Carrondo, The architecture of the binding site in redox protein complexes: implications for fast dissociation, Proteins 55 (2004) 603–612.
[10] P. Sétif, in: J.H. Golbeck (Ed.), Electron transfer from the bound iron–sulfur clusters to ferredoxin/flavodoxin: kinetic and structural properties of ferredoxin/flavodoxin reduction by photosystem I, Book Springer, Dordrecht, The Netherlands, 2006, pp. 439–454.
[11] P. Sétif, N. Fischer, B. Lagoutte, H. Bottin, J.D. Rochaix, The ferredoxin docking site of photosystem I, Biochim. Biophys. Acta 1555 (2002) 204–209.
[12] M. Medina, R. Abagyan, C. Gomez-Moreno, J. Fernandez-Recio, Docking analysis of transient complexes: interaction of ferredoxin-NADP$^+$ reductase with ferredoxin and flavodoxin, Proteins 72 (2008) 848–862.
[13] S.T. Rao, F. Shaffie, C. Yu, K.A. Satyshur, B.J. Stockman, J.L. Markley, M. Sundarlingam, Structure of the oxidized long-chain flavodoxin from *Anabaena* 7120 at 2 A resolution, Protein Sci. 1 (1992) 1413–1427.
[14] I. Nogues, L.A. Campos, J. Sancho, C. Gomez-Moreno, S.G. Mayhew, M. Medina, Role of neighboring FMN side chains in the modulation of flavin reduction potentials and in the energetics of the FMN:apoprotein interaction in *Anabaena* flavodoxin, Biochemistry 43 (2004) 15111–15121.
[15] A. Lostao, C. Gomez-Moreno, S.G. Mayhew, J. Sancho, Differential stabilization of the three FMN redox forms by tyrosine 94 and tryptophan 57 in flavodoxin from *Anabaena* and its influence on the redox potentials, Biochemistry 36 (1997) 14334–14344.
[16] S. Frago, G. Goñi, B. Herguedas, J.R. Peregrina, A. Serrano, I. Perez-Dorado, R. Molina, C. Gomez-Moreno, J.A. Hermoso, M. Martinez-Julvez, S.G. Mayhew, M. Medina, Tuning of the FMN binding and oxido-reduction properties by neighboring side chains in *Anabaena* flavodoxin, Arch. Biochem. Biophys. 467 (2007) 206–217.
[17] J.L. Casaus, J.A. Navarro, M. Hervas, A. Lostao, M.A. De la Rosa, C. Gomez-Moreno, J. Sancho, M. Medina, *Anabaena* sp. PCC 7119 flavodoxin as electron carrier from photosystem I to ferredoxin-NADP$^+$ reductase. Role of Trp(57) and Tyr(94), J. Biol. Chem. 277 (2002) 22338–22344.
[18] C. Walsh, J. Fisher, R. Spencer, D.W. Graham, W.T. Ashton, J.E. Brown, R.D. Brown, E.F. Rogers, Chemical and enzymatic properties of riboflavin analogues, Biochemistry 17 (1978) 1942–1951.
[19] J.D. Walsh, A.-F. Miller, Flavin reduction potential tuning by substitution and bending, J. Mol. Struct. (Teochem) 623 (2003) 185–195.
[20] D.R. Light, C. Walsh, Flavin analogs as mechanistic probes of adrenodoxin reductase-dependent electron transfer to the cholesterol side chain cleavage cytochrome P-450 of the adrenal cortex, J. Biol. Chem. 255 (1980) 4264–4277.
[21] T. Nishino, T. Nishino, L.M. Schopfer, V. Massey, Reactivity of chicken liver xanthine dehydrogenase containing modified flavins, J. Biol. Chem. 264 (1989) 6075–6085.
[22] L.M. Schopfer, A. Wessiak, V. Massey, Interpretation of the spectra observed during oxidation of p-hydroxybenzoate hydroxylase reconstituted with modified flavins, J. Biol. Chem. 266 (1991) 13080–13085.
[23] S. Ghisla, V. Massey, New flavins for old: artificial flavins as active site probes of flavoproteins, Biochem. J. 239 (1986) 1–12.
[24] K. Yorita, H. Misaki, B.A. Palfey, V. Massey, On the interpretation of quantitative structure–function activity relationship data for lactate oxidase, Proc. Natl. Acad. Sci. U.S.A. 97 (2000) 2480–2485.
[25] C.G. Genzor, A. Perales-Alcon, J. Sancho, A. Romero, Closure of a tyrosine/tryptophan aromatic gate leads to a compact fold in apo flavodoxin, Nat. Struct. Biol. 3 (1996) 329–332.
[26] D.E. Edmondson, G. Tollin, Chemical and physical characterization of the Shethna flavoprotein and apoprotein and kinetics and thermodynamics of flavin analog binding to the apoprotein, Biochemistry 10 (1971) 124–132.
[27] M. Rogner, P.J. Nixon, B.A. Diner, Purification and characterization of photosystem I and photosystem II core complexes from wild-type and phycocyanin-deficient strains of the cyanobacterium *Synechocystis* PCC 6803, J. Biol. Chem. 265 (1990) 6189–6196.
[28] M. Hervás, J.M. Ortega, J.A. Navarro, M.A. De la Rosa, H. Bottin, Laser flash kinetic analysis of *Synechocystis* PCC 6803 cytochrome c_6 and plastocyanin oxidation by Photosystem I, Biochim. Biophys. Acta 1184 (1994) 235–241.
[29] P. Mathis, P. Sétif, Near infra-red absorption spectra of the chlorophyll a cations and triplet state *in vivo*, Isr. J. Chem. 21 (1981) 316–320.
[30] K. Shin, K. Tagawa, D.I. Arnon, Crystallization of ferredoxin-TPN reductase and its role in the fhotosynthetic apparatus of chloroplasts, Biochem. Z. (1963) 338.
[31] S. Frago, M. Martinez-Julvez, A. Serrano, M. Medina, Structural analysis of FAD synthetase from *Corynebacterium ammoniagenes*, BMC Microbiol. 8 (2008) 160.
[32] M. Medina, M. Martinez-Julvez, J.K. Hurley, G. Tollin, C. Gomez-Moreno, Involvement of glutamic acid 301 in the catalytic mechanism of ferredoxin-NADP+ reductase from *Anabaena* PCC 7119, Biochemistry 37 (1998) 2715–2728.
[33] S.G. Mayhew, Potentiometric measurement of oxidation-reduction potentials, Methods Mol. Biol. 131 (1999) 49–59.
[34] M. Medina, M. Hervas, J.A. Navarro, M.A. De la Rosa, C. Gomez-Moreno, G. Tollin, A laser flash absorption spectroscopy study of *Anabaena* sp. PCC 7119 flavodoxin photoreduction by photosystem I particles from spinach, FEBS Lett. 313 (1992) 239–242.
[35] U. Muhlenhoff, P. Setif, Laser flash absorption spectroscopy study of flavodoxin reduction by photosystem I in *Synechococcus* sp. PCC 7002, Biochemistry 35 (1996) 1367–1374.
[36] M. Hervas, J.A. Navarro, A. Diaz, H. Bottin, M.A. De la Rosa, Laser-flash kinetic analysis of the fast electron transfer from plastocyanin and cytochrome c_6 to photosystem I. Experimental evidence on the evolution of the reaction mechanism, Biochemistry 34 (1995) 11321–11326.
[37] T.E. Meyer, Z.G. Zhao, M.A. Cusanovich, G. Tollin, Transient kinetics of electron transfer from a variety of c-type cytochromes to plastocyanin, Biochemistry 32 (1993) 4552–4559.
[38] K. Sigfridsson, Ö. Hansson, G.B. Karlsson, L. Baltzer, M. Nordling, L.G. Lundberg, Spectroscopic and kinetic characterization of the spinach plastocyanin mutant Tyr83-His: a histidine residue with a high pK value, Biochim. Biophys. Acta 1228 (1995) 28–36.
[39] M.J. Frisch, G.W. Trucks, H.B. Schlegel, G.E. Scuseria, M.A. Robb, J.R. Cheeseman, V.G. Zakrzewski, J.A. Montgomery, R.E. Stratmann and J.C. Burant. Gaussian, Inc., Pittsburgh PA 2003.
[40] C.L. Bayly, P. Cieplak, W.D. Cornell, P.A. Kollman, A well-behaved electrostatic potential based method sing charge restraints for deriving atomic charges: the RESP model, J. Phys. Chem. 97 (1993) 10269–10280.
[41] D.A. Case, T.E. Cheatham 3rd, T. Darden, H. Gohlke, R. Luo, K.M. Merz Jr., A. Onufriev, C. Simmerling, B. Wang, R.J. Woods, The AMBER biomolecular simulation programs, J. Comput. Chem. 26 (2005) 1668–1688.
[42] J. Wang, R.M. Wolf, J.W. Caldwell, P.A. Kollman, D.A. Case, Development and testing of a general amber force field, J. Comput. Chem. 25 (2004) 1157–1174.
[43] W.L. Delano, They PyMOL molecular graphics system, DeLano Scientific, San Carlos, CA, USA (2002) http://www.pymol.org.
[44] W. Humphrey, A. Dalke, K. Schulten, VMD—visual molecular dynamics, J. Mol. Graph. 14 (1996) 33–38.
[45] R.F. Anderson, Energetics of the one-electron reduction steps of riboflavin, FMN and FAD to their fully reduced forms, Biochim. Biophys. Acta 722 (1983) 158–162.
[46] S.G. Mayhew, The effects of pH and semiquinone formation on the oxidation-reduction potentials of flavin mononucleotide. A reappraisal, Eur. J. Biochem. 265 (1999) 698–702.
[47] F. Muller, V. Massey, Flavin–sulfite complexes and their structures, J. Biol. Chem. 244 (1969) 4007–4016.
[48] M.T. Stankovich, in: F. Müller (Ed.), Redox properties of flavins and flavoproteins, Book CRC Press, Inc., Boca Raton, Fl., 1991, pp. 401–425.
[49] K. Meimberg, B. Lagoutte, H. Bottin, U. Muhlenhoff, The PsaE subunit is required for complex formation between photosystem I and flavodoxin from the cyanobacterium *Synechocystis* sp. PCC 6803, Biochemistry 37 (1998) 9759–9767.
[50] J.J. van Thor, T.H. Geerlings, H.C. Matthijs, K.J. Hellingwerf, Kinetic evidence for the PsaE-dependent transient ternary complex photosystem I/Ferredoxin/Ferredoxin:NADP$^+$ reductase in a cyanobacterium, Biochemistry 38 (1999) 12735–12746.